

## Scaling Methodology Applied to Buckling of Sandwich Composite Cylindrical Shells

Uriol Balbin, Ines; Bisagni, Chiara; Schultz, Marc R.; Hilburger, Mark W.

**DOI**

[10.2514/1.J058999](https://doi.org/10.2514/1.J058999)

**Publication date**

2020

**Document Version**

Final published version

**Published in**

AIAA Journal: devoted to aerospace research and development

**Citation (APA)**

Uriol Balbin, I., Bisagni, C., Schultz, M. R., & Hilburger, M. W. (2020). Scaling Methodology Applied to Buckling of Sandwich Composite Cylindrical Shells. *AIAA Journal: devoted to aerospace research and development*, 58(8), 3680-3689. <https://doi.org/10.2514/1.J058999>

**Important note**

To cite this publication, please use the final published version (if applicable). Please check the document version above.

**Copyright**

Other than for strictly personal use, it is not permitted to download, forward or distribute the text or part of it, without the consent of the author(s) and/or copyright holder(s), unless the work is under an open content license such as Creative Commons.

**Takedown policy**

Please contact us and provide details if you believe this document breaches copyrights. We will remove access to the work immediately and investigate your claim.

# Scaling Methodology Applied to Buckling of Sandwich Composite Cylindrical Shells

Ines Uriol Balbin\* and Chiara Bisagni†

Delft University of Technology, 2629 HS Delft, The Netherlands  
and

Marc R. Schultz‡ and Mark W. Hilburger§

NASA Langley Research Center, Hampton, Virginia 23681

<https://doi.org/10.2514/1.J058999>

Studying buckling behavior of large shell structures through full-scale test articles can be complex and expensive. Therefore, reduced-scale structures are often preferred for investigating buckling behavior. However, designing reduced-scale structures that are representative of the full-scale structure can be difficult. An analytical scaling methodology for compression-loaded sandwich composite cylindrical shells based on the nondimensionalization of the buckling equations is presented herein. The methodology was used to develop scaled configurations that show similar buckling responses to the full-scale baseline configuration. Finite element analysis results showed that both a baseline and a scaled configuration buckled similarly, when the nondimensional stiffness, defined as the ratio between the nondimensional load and nondimensional displacement, was matched between the different scale models. Limitations of the methodology are discussed and are believed to be a result of neglecting the flexural anisotropy and the transverse shear compliance. A preliminary material failure assessment for the different scales is also considered.

## Nomenclature

$a_{ij}$	=	membrane compliance matrix
$D_{ij}$	=	bending stiffness matrix
$F$	=	nondimensional stress function
$G_{12}$	=	in-plane shear modulus, MPa
$G_{13}, G_{23}$	=	transverse shear moduli, MPa
$K$	=	nondimensional loading parameter, $N_{11} R^2 / \sqrt{D_{11} D_{22}}$
$L$	=	cylindrical shell length, mm
$M_{ij}$	=	nondimensional moments
$m$	=	number of axial half-waves
$N_{11}$	=	axial force resultant, $P / 2\pi R$ , N/mm
$n$	=	number of circumferential full waves
$P$	=	axial load, kN
$P_{CS}$	=	core shear crimping load, kN
$R$	=	cylindrical shell midsurface radius, mm
$t$	=	radial coordinate
$t_{core}$	=	sandwich core thickness, mm
$t_{facesheet}$	=	facesheet thickness, mm
$t_{ply}$	=	ply thickness, mm
$U$	=	nondimensional axial displacement, $u L / \sqrt{a_{11} a_{22} D_{11} D_{22}}$
$u$	=	axial displacement, mm
$V$	=	nondimensional circumferential displacement, $v R / \sqrt{a_{11} a_{22} D_{11} D_{22}}$
$v$	=	circumferential displacement, mm

$W$	=	nondimensional radial displacement, $w / \sqrt{a_{11} a_{22} D_{11} D_{22}}$
$w$	=	radial displacement, mm
$x$	=	axial coordinate
$Z_2$	=	Batdorf–Stein nondimensional parameter, $R / (\sqrt{12} \sqrt{a_{11} a_{22} D_{11} D_{22}})$
$z_1$	=	nondimensional axial coordinate, $x/L$
$z_2$	=	nondimensional circumferential coordinate, $R\theta/R$
$z_3$	=	nondimensional radial coordinate, $2t / (t_{core} + 2t_{facesheet})$
$\alpha_b$	=	nondimensional parameter, $(R/L) \sqrt{D_{11}/D_{22}}$
$\alpha_m$	=	nondimensional parameter, $(R/L) \sqrt{a_{22}/a_{11}}$
$\beta$	=	flexural orthotropy nondimensional parameter, $(D_{12} + 2D_{66}) / \sqrt{D_{11} D_{22}}$
$\delta_b$	=	flexural anisotropy parameter, $D_{26} / \sqrt{D_{11} D_{22}^3}$
$\gamma_b$	=	flexural anisotropy parameter, $D_{16} / \sqrt{D_{11} D_{22}^3}$
$\mu$	=	membrane orthotropy nondimensional parameter, $(2a_{12} + a_{66}) / (2\sqrt{a_{11} a_{22}})$
$\nu_b$	=	nondimensional generalized Poisson's ratio associated with bending, $D_{12} / \sqrt{D_{11} D_{22}}$
$\Theta$	=	angular coordinate
$\theta$	=	ply angle, deg

## Subscript

buck = lowest linear buckling load

## Superscripts

(b) = baseline  
(s) = scaled

## I. Introduction

SANDWICH composite structures with laminated facesheets and honeycomb core are often considered for space applications due to the high structural efficiency [1] that the use of sandwich composites can provide to, for instance, launch-vehicle shell structures. These launch-vehicle structures are often cylindrical shells that can be buckling critical. Therefore, the critical axial buckling load can be an important design consideration, and the buckling behavior must be well understood.

Presented as Paper 2018-1988 at the 2018 AIAA/ASCE/AHS/ASC Structures, Structural Dynamics, and Materials Conference, Kissimmee, FL, January 8–13, 2018; received 28 August 2019; revision received 13 March 2020; accepted for publication 26 March 2020; published online 8 May 2020. This material is declared a work of the U.S. Government and is not subject to copyright protection in the United States. All requests for copying and permission to reprint should be submitted to CCC at [www.copyright.com](http://www.copyright.com); employ the eISSN 1533-385X to initiate your request. See also AIAA Rights and Permissions [www.aiaa.org/randp](http://www.aiaa.org/randp).

\*Ph.D. Student, Faculty of Aerospace Engineering, Kluyverweg 1.

†Full Professor, Faculty of Aerospace Engineering, Kluyverweg 1. Associate Fellow AIAA.

‡Research Aerospace Engineer, Structural Mechanics and Concepts Branch, 8 West Taylor Street. Associate Fellow AIAA.

§Senior Research Engineer, Structural Mechanics and Concepts Branch, 8 West Taylor Street. Associate Fellow AIAA.

Shell buckling is an inherently nonlinear phenomenon where manufacturing imperfections can drastically reduce the buckling load. This reduction is usually accounted for in the design process by using buckling knockdown factors obtained from experimental data. A widely recognized source for these knockdown factors is NASA SP-8007 [2], which gives buckling knockdown factors for various shell types, including orthotropic shells and sandwich shells with isotropic facing sheets. The SP-8007 is widely used but provides limited information regarding composite shells and is believed to be overly conservative for many designs. Additionally, little laminated composite shell data were available in 1968 when NASA SP-8007 was written. Since then, sandwich shells in general and composite sandwich shells in particular have been studied by several authors. For example, Vinson [3] and Librescu and Hause [4] summarize much of the literature including numerical and experimental studies.

The NASA Shell Buckling Knockdown Factor project is working to better understand the buckling behavior of launch-vehicle shell structures and to update the knockdown factors for stiffened metallic and unstiffened sandwich composite structures [5,6]. New knockdown factors are expected to be less conservative and therefore result in a decrease in structural mass; this is particularly desirable in the development of launch vehicles because of the direct influence of mass on the performance and cost.

The study of the buckling behavior of large shell structures through full-size tests is complex and expensive. For this reason, reduced-scale structures are often preferred for the investigation of buckling behavior. For metallic structures, such scaled cylinders have already been proven effective for developing design guidelines [6]. However, scaling down representative large sandwich composite structures can be challenging because of the high number of parameters involved in the stiffness properties of the structure such as the thickness, the materials, and the ply orientations. The design of a scaled structure needs to be considered carefully in order to obtain a comparable result, and several approaches and methodologies have been taken to address this problem.

One approach consists of considering each possible scaled configuration on a case-by-case basis. A recent European Union project, New Robust Design Guideline for Imperfection Sensitive Composite Launcher Structures (DESICOS) had the goal of examining the imperfection sensitivity of large composite shell structures. The scaled configurations were chosen by an iterative process where the goal was to keep some geometric relations (i.e., radius-to-thickness ratio  $R/t$  and length-to-radius ratio  $L/R$ ) and the lowest eigenvalue equal to the original structure [7].

More formal methodologies have been developed as well. Among them, dimensional analysis was the first method used to design scaled structures [8]. The dimensional analysis reduces all the variables that intervene in the system and produces a series of independent dimensionless parameters; these parameters are considered the scaling laws. Sets of scaled structures are considered to have complete

similarity when all the independent dimensionless parameters are the same for both configurations. The main disadvantage of this methodology is the difficulty in identifying the scaling laws. Therefore, this methodology is not employed for problems with a large number of design parameters such as composite materials.

If the governing equations of the phenomena are known, another formal method for scaling is based on similarity between governing equations. This was shown by Rezaeepazhand et al. [9], who studied the case of laminated cylindrical shells under axial compressive load. This method avoids the difficulty of identifying the dimensionless parameters and is therefore powerful in obtaining complete and partial similarity laws for the design of scaled structures. The main advantage of this method is that the scaling laws are deduced directly from each parameter in the governing equations. The difficulty is in simultaneously fulfilling all the scaling laws while remaining within the design and manufacturing constraints. The consequence is that in most cases the scaled model that is produced fulfills only partially the similarity laws. For these cases, the lack of complete similarity limits the applicability of the results.

Finally, the use of nondimensional governing equations is also a scaling procedure, where the nondimensional parameters of the equations become the scaling laws. For instance, Hilburger et al. [10] used the nondimensional equations based on Reissner–Mindlin plate theory to obtain scaling laws for sandwich composite plates subjected to combined loads. The main advantage of this method is that the results of the buckling equations are also in nondimensional form and can be compared with the different scales.

The objective of the current study is to develop an analytical scaling methodology based on nondimensional governing equations for cylindrical shells under axial compression. This approach not only benefits from the use of scaling laws directly derived from the governing equations but also provides the framework to evaluate the response. Such a methodology was developed and then used to characterize the behavior of large sandwich composite cylindrical shells subjected to axial compression through scaled cylindrical shells that are computationally verifiable, testable in a laboratory, and ultimately applicable to specific full-scale structures.

## II. Scaling Methodology

The cylindrical structure that needs to be scaled, referred to as the baseline configuration, is a cylindrical sandwich composite shell with carbon fiber facesheets and aluminum honeycomb core. The result of the structural scaling, referred to as the scaled configuration, is also a cylindrical sandwich composite shell with the same facesheet and core materials. The two configurations, as well as considered geometric variables, are presented in Fig. 1. The dimensional ( $x, \Theta, t$ ) and nondimensional ( $z_1, z_2, z_3$ ) coordinates and the dimensional ( $u, v, w$ ) and nondimensional ( $U, V, W$ ) displacements are also depicted. The

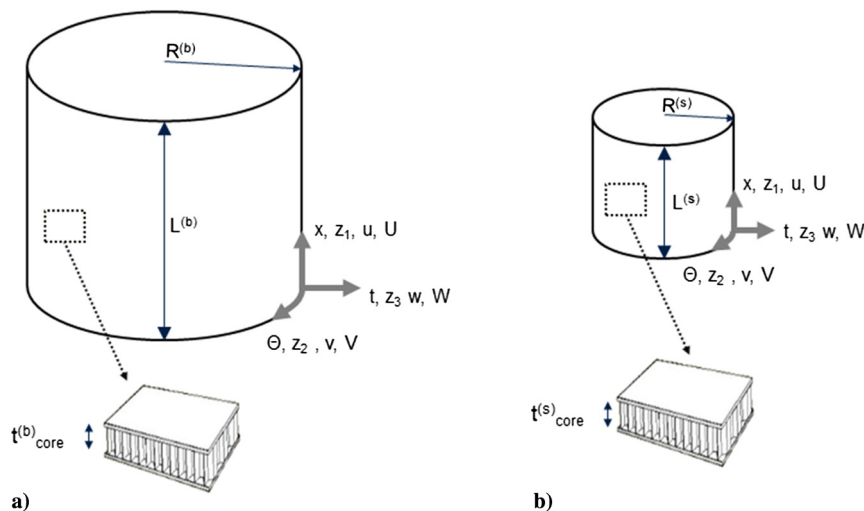


Fig. 1 Geometry and coordinate system: a) baseline configuration and b) scaled configuration.

**Table 1** Material properties

	$E_{11}$ , MPa	$E_{22}$ , MPa	$\nu$	$G_{12}$ , MPa	$G_{13}$ , MPa	$G_{23}$ , MPa	$t_{ply}$ , mm
Carbon fiber (IM7/8552 <sup>11</sup> )	149916	9370	0.36	5310	5310	2655	0.18
Aluminum honeycomb (3.1 pcf 1/8-5056-.0007)	6.7	6.7	0.30	1.5	138	310	—

stiffness properties of such composite structures can be varied by changing the facesheet stacking sequences, and in this study, stacking sequences that depend on only one variable, a ply angle  $\theta$  with respect to the axial direction ( $x, z_1$ ), are considered for the scaled cylinders. This consideration of a single ply angle as a variable presents the advantage that the facesheet stiffness properties are defined by a layup family and a single parameter. The drawback of using one angle parameter is that unconventional angles will be produced, which can lead to manufacturing and other complications.

The scaling procedure was applied to two baseline designs, denoted with the superscripts (b), each with radius  $R^{(b)}$  of 1202 mm and length  $L^{(b)}$  of 2305 mm, which results in the ratio  $R^{(b)}/L^{(b)} = 0.52$ . The facesheets are made of IM7/8552 carbon fiber whose mean properties [11] are reported in Table 1. The chosen baseline designs are simplified subscale launch-vehicle structures similar to those used as large-scale test articles in related NASA work [12]. Specifically, the stacking sequence of the facesheets is  $[60/-60/0]_s$  for the first baseline shell (baseline 1), and  $[30/-30/90/0]_s$  for the second shell (baseline 2). The aluminum honeycomb cores, whose properties are also reported in Table 1, have thicknesses  $t_{core}^{(b)}$  of 5.08 mm for baseline 1 and 7.62 mm for baseline 2.

The developed methodology was used to obtain scaled (s) configurations representative of the baseline structures. The geometry defined by  $R^{(s)}$  and  $L^{(s)}$  had to be determined. Additionally, the number of plies, the stacking sequence of the facesheets, and the core thickness  $t_{core}^{(s)}$  had to be decided. Two families of stacking sequences are considered for the facesheets, and with both families, the ply stacking sequence was a function of only one variable. These facesheet stacking sequence families are 1) a symmetric balanced four-ply laminate,  $[\theta/\theta/0/0]_s$ , and 2) a three-ply balanced unsymmetric laminate,  $[\theta/0/0/-\theta]_s$ .

Note that, though the second stacking sequence family is an unsymmetric laminate, when this stacking sequence is used for the facesheets in the sandwich cylinder, the resulting full sandwich shell is symmetric about the midsurface.

The scaling methodology is based on the nondimensional form of the Donnell–Mushtari–Vlasov buckling equations as defined by Nemeth [13,14] and specialized for use with compression-loaded circular cylinders by Schultz and Nemeth [15]. The buckling equations are formulated under the assumptions of small strains and neglect transverse-shear deformations and initial geometric imperfections. These last two assumptions may not be universally valid. The considered equations also treat the entire sandwich structure as a balanced and symmetric laminate, neglecting bend-twist anisotropy effects. With these considerations, the linearized nondimensional governing equations of compatibility and equilibrium, Eqs. (1) and (2), are compatibility equation:

$$\alpha_m^2 F_{,z_1 z_1 z_1 z_1} + \frac{1}{\alpha_m^2} F_{,z_2 z_2 z_2 z_2} + 2\mu F_{,z_1 z_1 z_2 z_2} - \sqrt{12} Z_2 W_{,z_1 z_1} = 0 \quad (1)$$

equilibrium equation:

$$\alpha_b^2 W_{,z_1 z_1 z_1 z_1} + \frac{1}{\alpha_b^2} W_{,z_2 z_2 z_2 z_2} + 2\beta W_{,z_1 z_1 z_2 z_2} + \sqrt{12} Z_2 F_{,z_1 z_1} - K W_{,z_1 z_1} = 0 \quad (2)$$

where  $\alpha_m, \mu, Z_2, \alpha_b, \beta$ , and  $K$  are nondimensional parameters defined by Eqs. (4–9),  $F$  is a nondimensional stress function, and  $W$  is the nondimensional radial displacement given by Eq. (3),

$$W = w / \sqrt[4]{a_{11} a_{22} D_{11} D_{22}} \quad (3)$$

where  $w$  is the radial displacement, the  $a_{ij}$  are membrane compliances, and the  $D_{ij}$  are bending stiffnesses. The subscripts  $z_1$  and  $z_2$  represent the derivatives in the axial and circumferential direction in the nondimensional coordinates, respectively.

Using the nondimensional parameters in Eqs. (1) and (2), the buckling response is not explicitly dependent on the geometric parameters. Rather, the response is formulated by the six nondimensional parameters presented in Eqs. (4–9) as reported in the literature [15], and the scaling laws are the nondimensional parameters in these equations. That is, the nondimensional parameters are used as the metrics to describe similarity, and the nondimensional buckling response described by Eqs. (1) and (2) of different cylinders with identical nondimensional parameters should be identical.

The first two parameters  $\mu$  and  $\beta$  depend only on the components of the in-plane compliance matrix and the bending stiffness matrix, respectively:

$$\mu = \frac{2a_{12} + a_{66}}{2\sqrt{a_{11} a_{22}}} \quad (4)$$

$$\beta = \frac{D_{12} + 2D_{66}}{\sqrt{D_{11} D_{22}}} \quad (5)$$

The parameter  $\alpha_m$  establishes a relation between the cylinder radius to length ratio  $R/L$  and the membrane compliances, while  $\alpha_b$  establishes a relation between  $R/L$  and the bending stiffnesses:

$$\alpha_m = \frac{R}{L} \sqrt[4]{\frac{a_{22}}{a_{11}}} \quad (6)$$

$$\alpha_b = \frac{R}{L} \sqrt[4]{\frac{D_{11}}{D_{22}}} \quad (7)$$

The Batdorf–Stein parameter  $Z_2$ , formally introduced by Nemeth [13], relates the radius with the membrane compliances and bending stiffnesses. The  $Z_2$  parameter is similar in character to a radius to the thickness ratio  $R/t$  because  $Z_2$  relates the shell radius to an equivalent thickness ( $\sqrt[4]{a_{11} a_{22} D_{11} D_{22}}$ ):

$$Z_2 = \frac{R}{\sqrt{12} \sqrt[4]{a_{11} a_{22} D_{11} D_{22}}} \quad (8)$$

Finally, the nondimensional loading parameter  $K$  relates the axial force resultant  $N_{11}$  with the bending stiffnesses and the midsurface shell radius,

$$K = \frac{N_{11} R^2}{\sqrt{D_{11} D_{22}}} = \frac{P}{2\pi R} \frac{R^2}{\sqrt{D_{11} D_{22}}} \quad (9)$$

where  $P$  is the total axial load.

The goal of the present study is to develop a methodology to design scaled configurations with nondimensional parameters that match the nondimensional parameters of the baseline configurations. The innovative aspect of the present methodology is that the parameters are decoupled, which allows each parameter to be calculated in a specific order. The parameter  $K$  is not part of the scaling methodology because  $K$  is solved to determine the lowest buckling load.

The first pair of parameters considered in the scaling methodology are the membrane orthotropy parameter  $\mu$ , from Eq. (4), and the flexural orthotropy parameter  $\beta$ , from Eq. (5). The two parameters relate the in-plane compliance matrix and the bending stiffness matrix parameters, are independent of geometry, and are a function of the material properties, the ply stacking sequence, and the core thickness. Two families of stacking sequences are considered:  $[\theta/-\theta]_s$  and  $[\theta/0/-\theta]$ , with a single ply angle  $\theta$  as the only variable. With these families of stacking sequences, the  $\mu$  and  $\beta$  parameters strongly depend only on the ply angle  $\theta$  (i.e.,  $\mu$  and  $\beta$  are insensitive to changes in core thickness and lightweight core material). This strong dependence on only ply angle is attributed to the fact that the thickness contributes to the numerator and denominator in similar ways in both Eqs. (4) and (5) and to the high in-plane stiffness of the facesheets when compared to typical core materials, which makes the influence of the core negligible. Therefore, the values of the parameters  $\mu$  and  $\beta$  are obtained as a function of the angle  $\theta$  for the two stacking sequence families shown in Fig. 2.

From the curves in Fig. 2, the angles required for each stacking sequence in order to maintain the baseline values of  $\mu^{(b)}$  and  $\beta^{(b)}$  are obtained. The value of  $\mu^{(b)}$  is 1 for baseline 1 and 1.51 for baseline 2. The value of  $\beta^{(b)}$  is 1 for baseline 1 and 0.78 for baseline 2. For each stacking sequence, the values of the angle necessary to match  $\mu^{(b)}$  are essentially the same as those necessary to match  $\beta^{(b)}$ . Note that for the considered laminate families there are two possible angles that yield equivalent membrane and flexural orthotropy parameters and therefore two possible configurations for the scaled cylindrical shells. Herein, the two configurations obtained from baseline 1 will be referred to as “scaled 1.1” and “scaled 1.2” for the first family  $[\theta/-\theta]_s$  and “scaled 1.3” and “scaled 1.4” for the second family  $[\theta/0/-\theta]$ . Similarly, the two configurations obtained from baseline 2 will be referred to as “scaled 2.1” and “scaled 2.2” for the first family  $[\theta/-\theta]_s$  and “scaled 2.3” and “scaled 2.4” for the second family  $[\theta/0/-\theta]$ . This labeling scheme can be seen in Fig. 3.

The next parameters to evaluate are  $\alpha_m^{(b)}$  [Eq. (6)] and  $\alpha_b$  [Eq. (7)]. Both of these parameters are a function of the ratio  $R/L$ . Both  $\alpha_m$  and  $\alpha_b$  are also influenced by the ply angle  $\theta$  and the core thickness  $t_{\text{core}}$ . However, the ply angles are determined in the previous step, and the core-thickness influence is negligible. Therefore, the parameters  $\alpha_m$  and  $\alpha_b$  can be determined solely by  $R/L$  as shown in Figs. 4 and 5 for baseline 1 and baseline 2, respectively, where the relationships for the scaled layouts are presented.

It is seen for a given facesheet stacking sequence and for a given ratio  $R/L$  that  $\alpha_m$  and  $\alpha_b$  are essentially equal and that the relationships between the  $\alpha_m$  and  $\alpha_b$  parameters and  $R/L$  are linear. This means that for each value of the  $\alpha_m$  and  $\alpha_b$  parameters a single solution for the  $R/L$  can be found. The ratio  $R/L$ , reported in Table 2, is important, and the value raises concerns of possible global bending if the cylinder is relatively long, while the influence of the boundary conditions can change the buckling response and the imperfection sensitivity when the cylinder is relatively short. Note that the  $R/L$  for scaled 1.1, 1.2, and 1.3 is quite different from  $R/L$  of baseline 1. The same  $R/L$  trend occurred for scaled 2.1, 2.2, and 2.3, which have

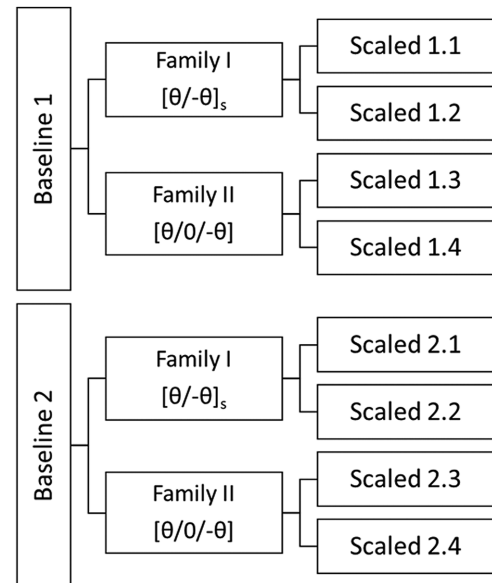


Fig. 3 Baseline and scaled configurations notation.

$R/L$  quite different from baseline 2. In particular, the  $R/L$  is approximately one-third for scaled 1.1, 1.3, 2.1, and 2.3, and the  $R/L$  is near unity for scaled 1.2 and 2.2. However, for scaled 1.4 and 2.4, the  $R/L$  is similar (within 20%) to their respective baseline.

The final parameter to evaluate is  $Z_2$  [Eq. (8)], which is a function of the radius, the axial and circumferential membrane compliances, and the bending stiffnesses. Given that the facesheet stacking sequence and  $R/L$  for the scaled configurations have been downselected, the baseline value of  $Z_2$  can be maintained in the scaled configurations with the right combination of radius  $R$  and core thickness  $t_{\text{core}}$ . However, available laboratory testing equipment constrains the upper bound for  $R$ , and the minimum manufacturable core thickness constrains the lower bound for  $t_{\text{core}}$ . In this study, the radius for all the scaled configurations is fixed and equal to 400 mm (33% of baseline) because this is a convenient size to be tested in many load frames. The variation of  $Z_2$  as a function of core thickness is depicted in Fig. 6, and the value of  $Z_2$  is obtained by selecting the core thickness of the scaled shell. As observed in Fig. 6 and reported in Table 2, the selected values of  $t_{\text{core}}$ , within the facesheet stacking sequence family  $[\theta/-\theta]_s$ , are essentially the same. For example, the core thickness difference within facesheet stacking sequence family  $[\theta/0/-\theta]$  is less than 1% as reported in Table 2. Notice also that the influence of the facesheet stacking sequence family on  $Z_2$  decreases as the desired value of  $Z_2$  decreases and as the core thickness increases. The scaled configurations with all the necessary variables, facesheet layup, length, and core thickness, are reported in Table 2.

For the scaled configurations to be tested in a laboratory-scale setting, certain manufacturing and laboratory equipment constraints

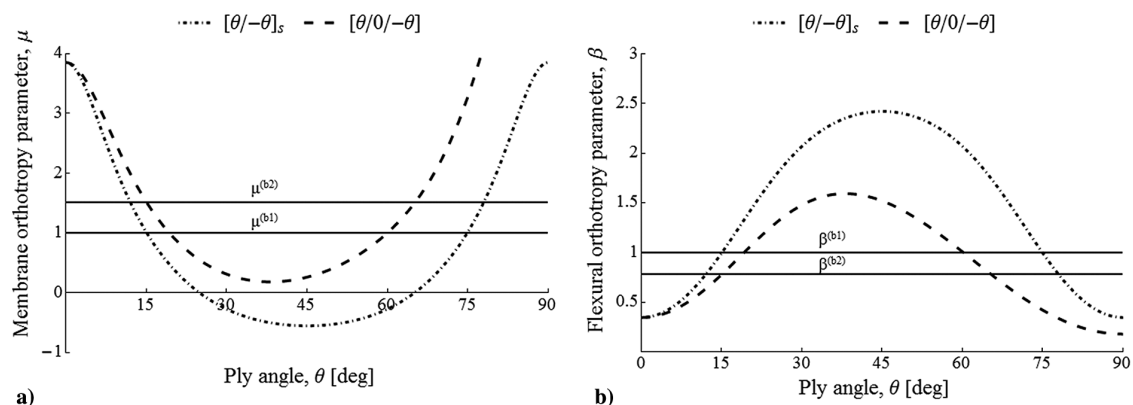


Fig. 2 Orthotropy parameters: a) membrane  $\mu$  and b) flexural  $\beta$  vs ply angle  $\theta$  for scaled facesheet stacking sequences  $[\theta/-\theta]_s$  and  $[\theta/0/-\theta]$ .

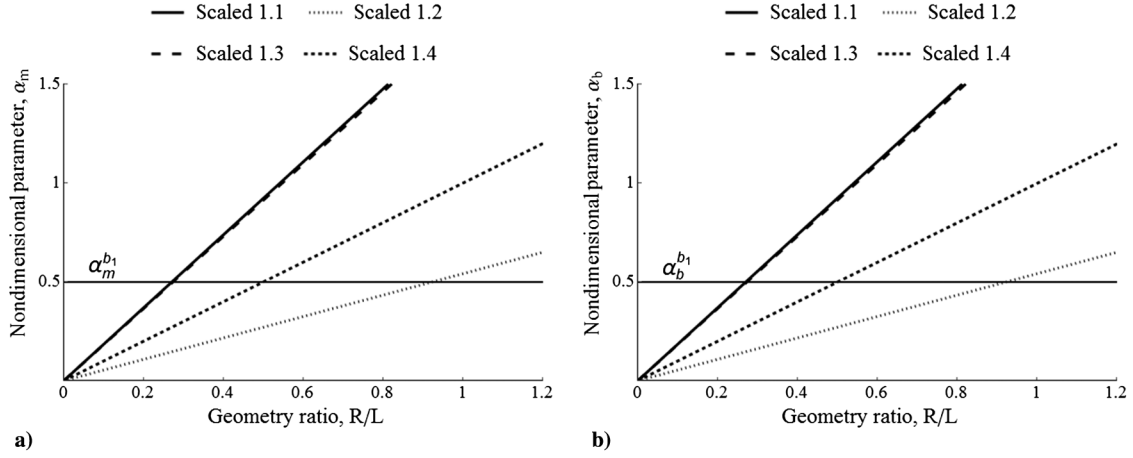


Fig. 4 Parameters: a)  $\alpha_m$  and b)  $\alpha_b$  vs  $R/L$  for scaled facesheet stacking sequences for baseline 1  $[60 - 60/0]_s$ .

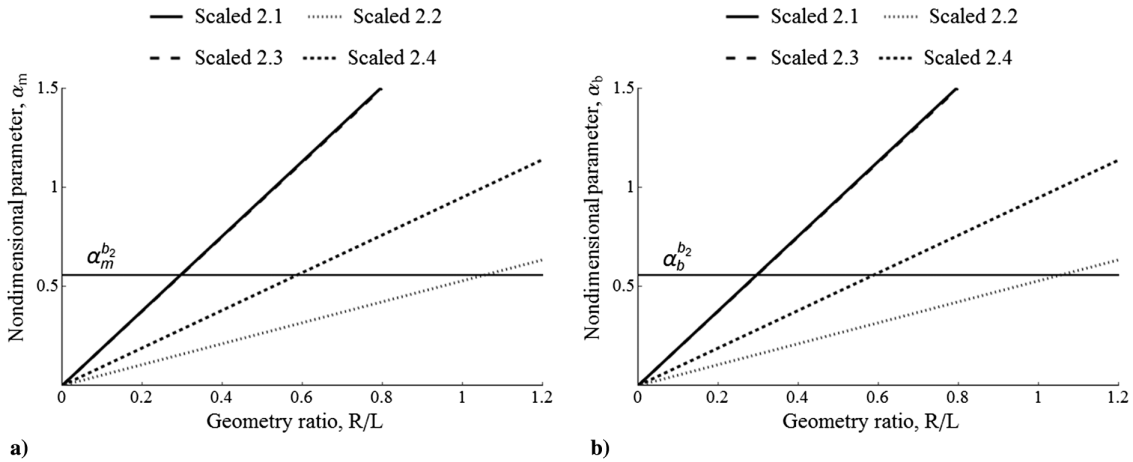


Fig. 5 Parameters: a)  $\alpha_m$  and b)  $\alpha_b$  vs  $R/L$  for scaled facesheet stacking sequences for baseline 2  $[30/-30/90/0]_s$ .

apply. The obtained scaled configurations should also have dimensions that fit in typical laboratory test equipment. Thus, restrictions in length, radius, and strength can prevent the testing of some of these configurations in a laboratory setting. The values of the thickness are very small and might not be possible for the considered core materials. The minimum core thickness manufacturable is closely connected not only to the core material, in this case aluminum honeycomb, but also to the fabrication technology and the tolerances required.

The nondimensional parameters for all scaled configurations of both baselines are reported in Table 3. One can see that  $\alpha_m$ ,  $\alpha_b$ , and  $Z_2$  match the associated baseline parameters identically. Regarding  $\mu$  and  $\beta$  parameters, the scaled 1.3, 1.4, 2.3, and 2.4 deviated from the

associated baseline more than the scaled 1.1, 1.2, 2.1, and 2.2. The parameter  $\beta$  deviated by the highest percentages of any of the parameters, up to 12%, for scaled 2.4. These results indicate that the  $[\theta/-\theta]_s$  family scales more precisely by exhibiting less variability in parameters than the  $[\theta/0/-\theta]$  family.

### III. Flexural Anisotropy Effects

As described thus far, the scaled configurations are considered similar to the baseline if they have equal nondimensional parameters. However, the considered nondimensional equations are formulated neglecting bend-twist anisotropy and flexural anisotropy. These effects are represented in the constitutive relations [Eq. (10)] by matrix elements that relate the nondimensional bending moments ( $M_{11}$  and  $M_{22}$ ) with the twisting curvature ( $\partial^2 W/\partial z_1 \partial z_2$ ) and by matrix elements that relate the nondimensional twisting moment ( $M_{12}$ ) with the bending curvature in the axial  $\partial^2 W/\partial z_1^2$  and radial directions  $\partial^2 W/\partial z_2^2$ . The full constitutive equations have additional nondimensional parameters derived by Nemeth [14] for symmetric laminated shells,

$$\begin{bmatrix} M_{11} \\ M_{22} \\ M_{12} \end{bmatrix} = \begin{bmatrix} \alpha_b^2 & \nu_b & -\gamma_b \alpha_b \\ -\nu_b & \frac{1}{\alpha_b^2} & -\delta_b/\alpha_b \\ -\gamma_b \alpha_b & -\delta_b/\alpha_b & \frac{\beta + \nu_b}{2} \end{bmatrix} \begin{bmatrix} \frac{\partial^2 W}{\partial z_1^2} \\ \frac{\partial^2 W}{\partial z_2^2} \\ 2 \frac{\partial^2 W}{\partial z_1 \partial z_2} \end{bmatrix} \quad (10)$$

where the nondimensional Poisson ratio  $\nu_b$  is

Table 2 Geometry of baseline and scaled configurations

Designation	Layup	$R/L$	Length, mm	$t_{\text{core}}$ , mm
Baseline 1	$[60/-60/0]_s$	0.52	2305	5.08
Scaled 1.1	$[15/-15]_s$	0.28	1445	1.30
Scaled 1.2	$[75/-75]_s$	0.95	410	1.30
Scaled 1.3	$[19/0/-19]$	0.28	1430	1.50
Scaled 1.4	$[60/0/-60]$	0.52	770	1.50
Baseline 2	$[30/-30/90/0]_s$	0.52	2305	7.62
Scaled 2.1	$[12/-12]_s$	0.31	1300	2.28
Scaled 2.2	$[78/-78]_s$	1.15	350	2.28
Scaled 2.3	$[15/0/-15]$	0.32	1250	2.49
Scaled 2.4	$[65/0/-65]$	0.62	645	2.47

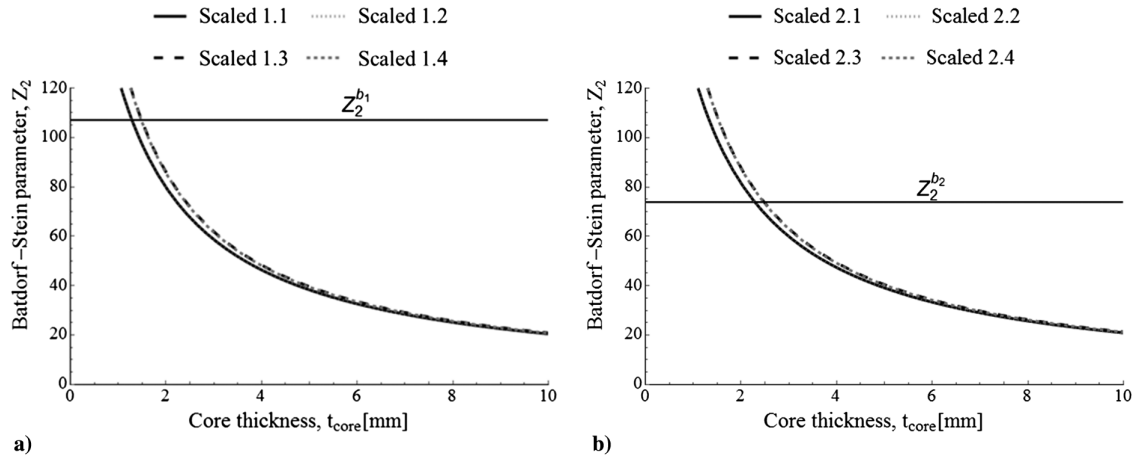


Fig. 6 Batdorf–Stein parameter  $Z_2$  as function of core thickness  $t_{\text{core}}$  for a) baseline 1 and b) baseline 2.

$$\nu_b = \frac{D_{12}}{\sqrt{D_{11}D_{22}}} \quad (11)$$

And the nondimensional flexural orthotropy parameters are

$$\gamma_b = \frac{D_{16}}{\sqrt[4]{D_{11}^3 D_{22}}} \quad (12)$$

$$\delta_b = \frac{D_{26}}{\sqrt[4]{D_{11} D_{22}^3}} \quad (13)$$

To verify the assumption that flexural anisotropy has a negligible effect on the response, the elements  $\delta_b/\alpha_b$  and  $\gamma_b\alpha_b$  are evaluated and should be smaller than the other elements of the matrix. Therefore, they have been compared to the lowest-value element of the matrix,

which is  $\alpha_b^2$ . This condition is expressed mathematically in Eqs. (14) and (15):

$$O(\delta_b/\alpha_b) \ll O(\alpha_b^2) \quad (14)$$

$$O(\gamma_b\alpha_b) \ll O(\alpha_b^2) \quad (15)$$

Hence, the ratios of the elements  $\delta_b/\alpha_b$  and  $\alpha_b\gamma_b$  with respect to the element  $\alpha_b^2$  should be as small as possible. For the baseline designs, the ratio is under 1%. However, these ratios are higher for all scaled designs compared to the baseline ratios, as reported in Table 4. The flexural anisotropy influence is stronger in the scaled configurations that derive from baseline 1. The influence is highest in the facesheet stacking sequences of the  $[\theta/0/-\theta]$  family. To reduce the anisotropy effects in the considered designs, scaled configurations 1.3, 1.4, 2.3, and 2.4 are removed from further consideration as scaled configurations.

#### IV. Methodology Verification

The methodology described allows one to obtain scaled configurations that have nondimensional parameters [Eqs. (4–9)] similar to the baseline configuration. The goal of scaling is to obtain scaled configurations that have a buckling response that is representative of the baseline configuration. The characteristics of buckling behavior compared herein are the buckling load, the buckling mode shape, the load-displacement curve, and the postbuckling shape.

Initially, the buckling loads and modes are calculated analytically with the procedure described by Schultz and Nemeth [15], from the governing equations [Eqs. (1) and (2)], assuming solutions for  $W$  and  $F$  in the form of double sine series. Eigenvalue analysis is then applied to solve for the lowest buckling value of  $K$ ,  $K_{\text{buck}}$ , and the buckling mode is described by the number of axial half-waves  $m$  and the number of circumferential full waves  $n$ . The boundary conditions used in the present study are simply supported with no radial or circumferential displacements and have zero bending moment at  $z_1 = 0$  and  $z_1 = 1$ . The obtained buckling loads and modes are reported in Table 5. The buckling mode for all scaled configurations matches the respective baseline buckling mode. The values of  $K_{\text{buck}}$  for all four scaled versions match the respective baseline values within 0.5%. For reference, the buckling loads  $P_{\text{buck}}$  calculated according to Eq. (9) are also shown in the third column of Table 5. The scaled buckling loads are also within the load range that a standard laboratory testing machine can apply (1500–2500 kN). This is relevant because the ultimate desire for these structures is the ability to test them using typical laboratory equipment.

The analytical buckling load calculation described leads to the same results as the formula reported by Vinson and Sierakowski [16]. Indeed, both formulations neglect the transverse shear compliance effects in the core. This was considered a reasonable hypothesis due to the relatively small thickness of the core. However, to evaluate

Table 3 Nondimensional parameters of baseline and scaled configurations

Designation	$\mu$	$\beta$	$\alpha_m$	$\alpha_b$	$Z_2$
Baseline 1	1.00	1.00	0.52	0.52	106.5
Scaled 1.1	1.01	0.99	0.52	0.52	106.5
Scaled 1.2	1.01	0.99	0.52	0.52	106.5
Scaled 1.3	1.03	0.99	0.52	0.52	106.5
Scaled 1.4	1.00	1.01	0.52	0.52	106.5
Baseline 2	1.46	0.79	0.60	0.60	74.1
Scaled 2.1	1.52	0.78	0.60	0.60	74.1
Scaled 2.2	1.52	0.78	0.60	0.60	74.1
Scaled 2.3	1.52	0.82	0.60	0.60	74.1
Scaled 2.4	1.49	0.89	0.60	0.60	74.1

Table 4 Flexural anisotropy terms of baseline and scaled configurations

Designation	Layup	$(\delta_b/\alpha_b)/\alpha_b^2, \%$	$\alpha_b\gamma_b/\alpha_b^2, \%$
Baseline 1	$[60/-60/0]_s$	0.73	0.55
Scaled 1.1	$[15/-15]_s$	9.77	0.98
Scaled 1.2	$[75/-75]_s$	3.60	2.64
Scaled 1.3	$[19/0/-19]$	86.72	12.22
Scaled 1.4	$[60/0/-60]$	42.43	31.20
Baseline 2	$[30/-30/90/0]_s$	0.67	0.11
Scaled 2.1	$[12/-12]_s$	2.47	0.25
Scaled 2.2	$[78/-78]_s$	0.71	0.87
Scaled 2.3	$[15/0/-15]$	31.01	3.87
Scaled 2.4	$[65/0/-65]$	12.73	16.31

**Table 5 Buckling load and buckling mode**

Designation	Axial half waves $m$	Circumferential full waves $n$	Lowest nondimensional loading parameter $K_{buck}$	Buckling load $P_{buck}^a$ kN	Buckling load $P_{buck}^b$ kN
Baseline 1	12	1	738	5075	4691
Scaled 1.1	12	1	739	670	611
Scaled 1.2	12	1	739	670	557
Baseline 2	4	8	446	8868	8270
Scaled 2.1	4	8	446	869	832
Scaled 2.2	4	8	446	869	762

<sup>a</sup>Schultz and Nemeth formulation [15].

<sup>b</sup>Reese and Bert formulation [17].

effects of transverse shear compliance, the results are compared to the formulation of Reese and Bert [17] that considers the transverse shear stiffnesses in the core  $G_{13}$  and  $G_{23}$ . As shown in Table 1, the transverse shear stiffnesses are significantly higher than the core in-plane shear stiffness  $G_{12}$ . The Reese and Bert formulation includes other assumptions and simplifications such as neglecting the in-plane core stiffness. Nevertheless, the comparison is an indication of the influence of the transverse-shear effects that are ignored in the present work.

As reported in Table 5, the buckling loads calculated from the two formulations differ significantly at both the baseline and scaled sizes. Specifically, the scaled 1.2 and 2.2 configurations show the highest differences in buckling load calculated from the two formulations; these differences are 17 and 12%, respectively. This difference leads one to consider that the inclusion of transverse-shear compliance could be included in the methodology to improve results; this would require extending the nondimensional framework to include the transverse shear effect. For the purposes of the current study, the scaled 1.1 and 2.1 configurations are chosen for further examination herein because the buckling loads calculated from the two formulations showed a relatively small difference.

The scaled 1.1 and 2.1 configurations are next considered with finite element analysis. Finite element models of the baseline and scaled configurations are generated using the commercial general-purpose finite element code Abaqus [18]. Since the considered sandwich shells

are relatively thin with thin cores, modeling the core as a layer in a laminated shell [19,20] was considered reasonable. Thus, S4R reduced-integration four-noded shell elements are used in the finite element analysis. The scaled model uses elements of approximately  $10 \times 10$  mm, and the baseline model uses elements of approximately  $30 \times 30$  mm; both were demonstrated to be converged mesh densities by comparing the linear buckling loads and mode shapes. The baseline model has 77 elements in the axial direction and 252 elements in the circumferential direction. The scaled 1.1 model has 134 elements in the axial direction and 251 elements in the circumferential direction, and the scaled 2.1 model has 125 elements in the axial direction and 251 elements in the circumferential direction. The buckling equations proposed considered simply supported conditions, so the numerical analyses used simply supported boundary conditions with all displacements fixed at both ends of the shells, except free axial translation allowed along the loaded edge. Two different analysis types were performed. First, a linear buckling analysis was conducted, and the first eigenmodes are compared in Fig. 7. Baseline 1 and scaled 1.1 show an axisymmetric pattern, while both baseline 2 and scaled 2.1 show a checkerboard pattern, which indicates that the eigenmode comparison is imperfect in this case. Second, an implicit nonlinear dynamic analysis was performed applying top edge displacement control with a velocity of 0.1 mm/s for baseline shells and 0.01 mm/s for scaled shells.

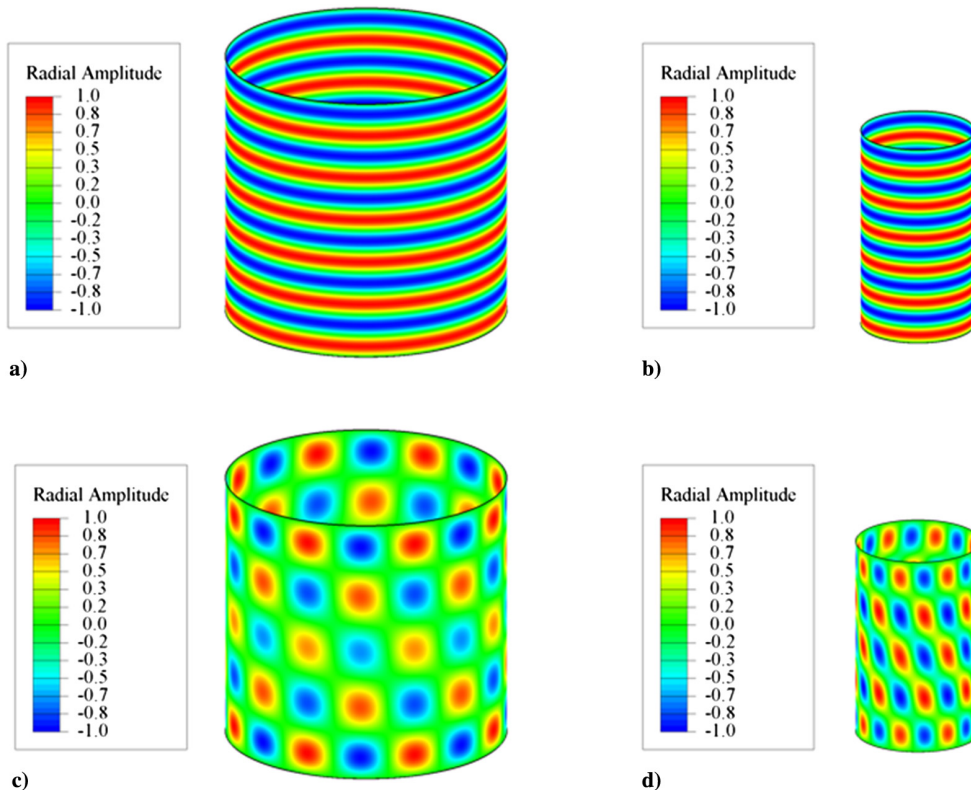


**Fig. 7 First linear buckling mode: a) baseline 1, b) scaled 1.1, c) baseline 2, and d) scaled 2.1.**

**Table 6 Comparison of analytical and finite element buckling loads**

Designation	Analytical buckling load $P_{\text{buck}}^a$ , kN	Finite element linear buckling load, kN	Finite element nonlinear dynamic buckling load, kN
Baseline 1	4691	4243	4061
Scaled 1.1	611	573	537
Baseline 2	8270	7918	7721
Scaled 2.1	832	809	767

<sup>a</sup>Reese and Bert formulation [17].

The analytical and finite element buckling loads are given in Table 6. The differences between the analytical and finite element buckling loads are 8.22 and 3.44% for baselines 1 and 2 and 6.30 and 2.75% for the scaled 1.1 and scaled 2.1, respectively. These differences are believed to be primarily due to assumptions that are made in the Reese and Bert [17] formulation, specifically in neglecting the anisotropy effects and the in-plane core stiffness.

The predicted load-displacement curves of the baseline and scaled configurations are shown in Fig. 8. The load of baseline 1 is 7.6 times higher than the load for scaled 1.1, whereas the load of baseline 2 is 10.1 times higher than the load for scaled 2.1. Regarding the displacement, both baseline structures reach the buckling load at 11.0 mm. The scaled 1.1 buckles at 1.9 mm, while scaled 2.1 reaches the buckling load at 2.2 mm. There is a nonlinear response before the buckling event in all cases that is more pronounced in the baseline models than in the scaled models. It is believed that this nonlinear response is related to large widespread axisymmetric prebuckling deformations that are observed in these analysis results.

The nondimensional load-displacement curves represent more accurately the similarity between configurations. The nondimensional load has already been discussed and described in Eq. (9); however, a nondimensional displacement needs to be established. According to the nondimensionalization methodology [14,15], the nondimensional axial displacement  $U$  can be calculated as described in Eq. (16),

$$U = \frac{uL}{\sqrt{a_{11}a_{22}D_{11}D_{22}}} \quad (16)$$

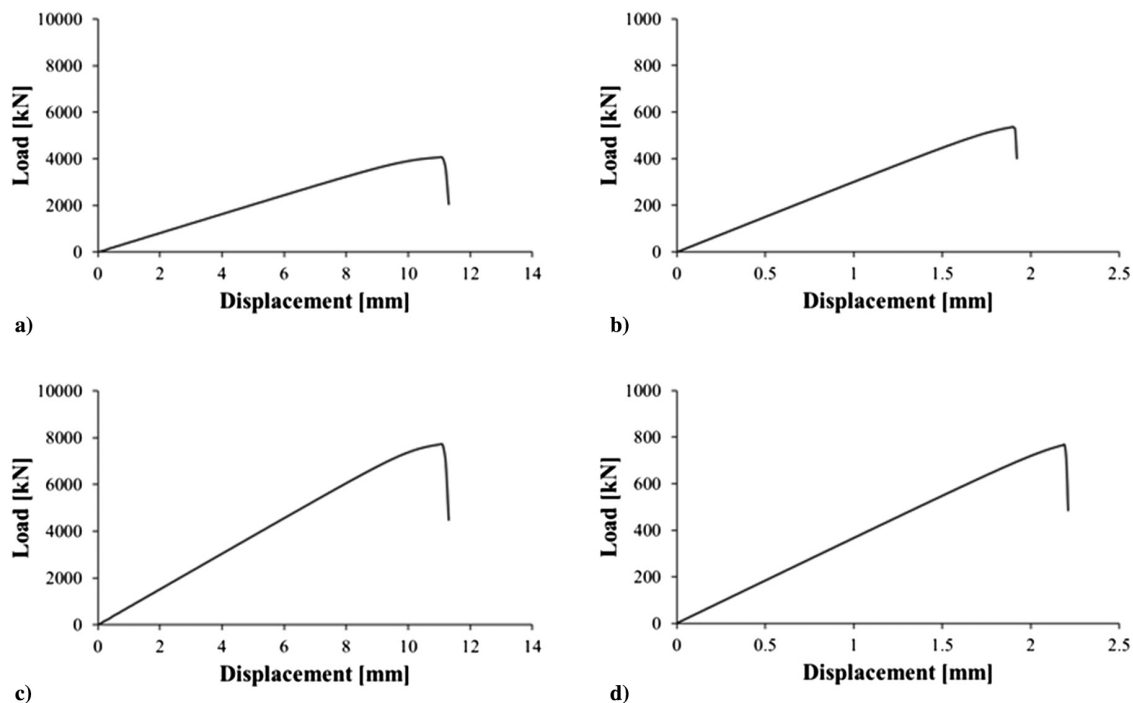


**Fig. 8 Load-displacement curves from finite element analysis: a) baseline 1, b) scaled 1.1, c) baseline 2, and d) scaled 2.1.**

where  $u$  is the axial displacement,  $L$  is the free axial length of the shell, and the  $a_{ij}$  and  $D_{ij}$  are the analytically calculated membrane compliances and bending stiffnesses, respectively. This formulation of nondimensional displacement implies that the errors in the anisotropy assumptions and transverse shear are carried to the nondimensional comparison. In Fig. 9, both baseline cylindrical shells and their scaled configurations are compared, and it is seen that the nondimensional stiffnesses for the baseline configurations and their corresponding scaled configurations are similar.

The differences at buckling between the baseline 1 and scaled 1.1 are 0.37% for the nondimensional load and 2.27% for the nondimensional displacement. The differences at buckling between the baseline 2 and scaled 2.1 are 3.88% for the nondimensional load and 1.34% for the nondimensional displacement. Nevertheless, the nondimensional stiffness calculated as the ratio of nondimensional load and the nondimensional displacement is matched for the baseline and the scaled models as shown in Table 7; between the baseline 1 and scaled 1.1 configurations, the difference in nondimensional stiffness is 2.70%, and for the baseline 2 and scaled 2.1, the difference in nondimensional stiffness is 2.51%.

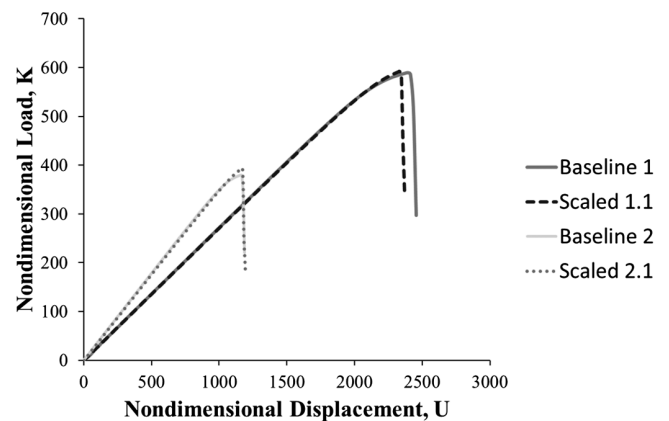


**Fig. 9 Nondimensional load-displacement curves of baseline and scaled.**

**Table 7 Numerical nondimensional load, displacement, and stiffness**

Designation	Nondimensional load $K$	Nondimensional displacement $U$	Nondimensional stiffness
Baseline 1	590	2390	0.247
Scaled 1.1	592	2336	0.253
Baseline 2	379	1156	0.328
Scaled 2.1	394	1171	0.336

**Table 8 Sandwich composite failure prediction**

Designation	Facesheet critical strains at incipient buckling [ $\mu\epsilon$ ]	Shear crimping critical load, kN
Baseline 1	8786	24,158
Scaled 1.1	2012	4503
Baseline 2	5236	33,874
Scaled 2.1	2374	3864

**V. Preliminary Failure Criteria Assessment**

Failure is investigated for the considered configurations in this section. Depending on the geometry and the loading, different failure modes can become critical for different sandwich structures. Even though the current methodology does not aim to scale material failures, material failure must occur after the buckling event in order to experimentally confirm the scaling process for buckling. For this reason, some of the relevant sandwich structure failure loads are discussed and compared for the baseline and the scaled configurations. It should be noted that the failure assessment discussed herein is only preliminary, and a more detailed finite element analysis should be performed to check if the assumptions regarding the modeling of the core are correct before manufacturing and testing.

To consider facesheet failure, the facesheet strains at incipient buckling are analyzed. The fiber-direction strains from the most critical ply of the inner facesheet at incipient buckling are calculated by finite element dynamic analysis and are reported in Fig. 10. The most critical ply varies in each configuration. For both scaled 1.1 and scaled 2.1, the most critical ply is the innermost ply, whereas for baseline 1, it is the third ply (0°), and for baseline 2, it is the fourth ply (0°) from the inside. The figures are shown with the deformation amplified by a factor of 20. There is a concentration of the strains in the edges of the shell for all cases. The predicted minimum strain values are reported in Table 8. These scaled-configuration buckling strains are below typical failure strains for IM7/8552, so by this measure, both scaled designs appear to be good candidates for effective buckling test articles.

Next, shear crimping is analyzed as the core can fail due to low core shear modulus, or due to thin facesheets, or both. To consider this type of failure, the formula presented by Reese and Bert Eq. (17) is used,

$$P_{CS} = 2\pi R \frac{G_{13}(t_{\text{facesheet}} + t_{\text{core}})^2}{t_{\text{core}}} \tag{17}$$

where  $R$  is the cylindrical shell midsurface radius,  $G_{13}$  is the core transverse shear moduli,  $t_{\text{facesheet}}$  is the facesheet thickness, and  $t_{\text{core}}$  is the core thickness. The load values corresponding to shear crimping are reported in Table 8, and they are higher than the values of buckling load reported in Table 5; therefore, shear crimping should not occur before buckling. Considering facesheet strain and shear crimping are simple checks, but other failure modes should also be checked before fabrication and testing of sandwich composite test articles such as these.

**VI. Conclusions**

A scaling methodology for the buckling of sandwich composite cylindrical shells is described. The methodology is based on the nondimensionalization of the buckling equations and the study of the nondimensional parameters. To simplify the number of parameters involved, stacking sequences that are determined by a single ply angle were chosen, and the sandwich structures are considered balanced and symmetric. This allowed the scaling to be reduced to a three-step process: first, the facesheet ply angle  $\theta$  is determined, second, the geometry ratio  $R/L$  is determined, and finally the sandwich core thickness  $t_{\text{core}}$  is determined. Through this process, scaled configurations can be found with the same nondimensional parameters as those of the baseline configurations, which reproduce similar buckling responses.

The developed methodology was used to find scaled designs for two baseline structures representative of launch vehicle structures.

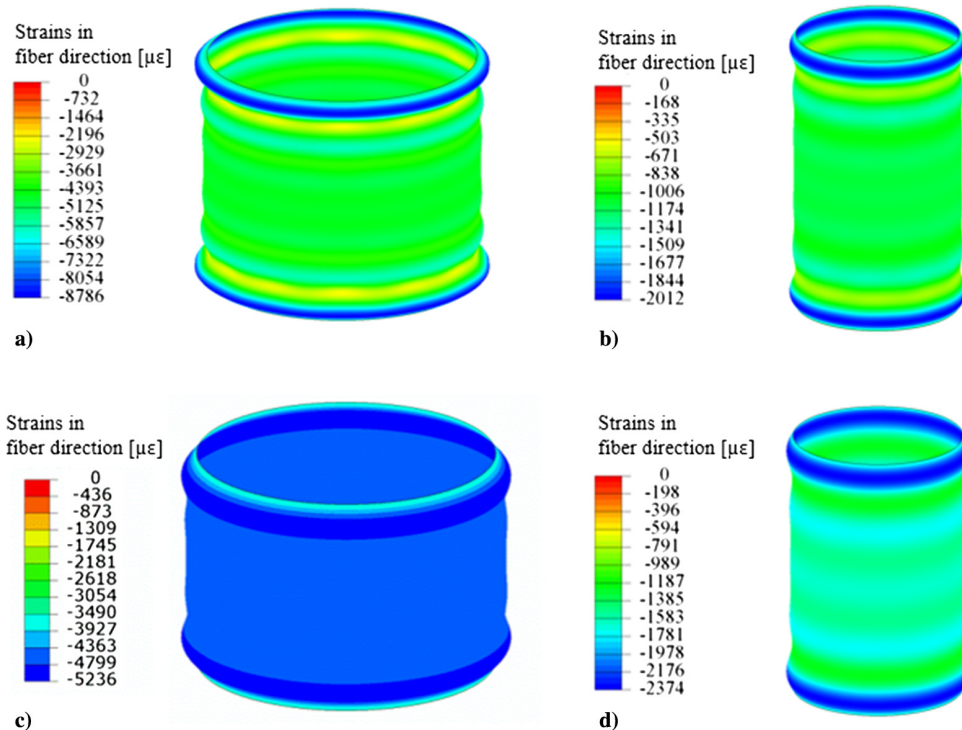


**Fig. 10 Fiber-direction strains at the highest prebuckling load of most critical ply: a) baseline 1, b) scaled 1.1, c) baseline 2, and d) scaled 2.1.**

The obtained scaled configurations have dimensions and buckling loads that can be applied with typical laboratory test equipment [21]. The studied cases have a small core thickness; thus, the considered core materials may not be viable due to manufacturing constraints.

The buckling responses of the baseline and scaled configurations were compared analytically and numerically. The scaled analytical buckling modes were found to be identical, and the scaled analytical nondimensional loading parameter  $K$  at buckling was within 0.5% for both baseline designs.

The applicability of the methodology is limited by two initial simplifications: ignoring the transverse-shear deformations and the flexural anisotropy parameters. The fact that these are neglected can explain some of the differences with the results of the finite element analyses. Extending the methodology to include the transverse-shear and flexural anisotropy is expected to extend the applicable range.

Finite element analysis was used to predict the scaled configurations results using the software Abaqus. From the analysis model, the dimensional and nondimensional load-displacement curves were compared between baseline and scaled cylindrical shells. For both cases, the difference of the nondimensional load and nondimensional displacement were less than 10%. The agreement was better in the case in which there is a lower transverse shear influence. Prebuckling strains and core shear crimping were also calculated and were predicted not to cause failures before buckling for the scaled configurations.

### Acknowledgments

The research presented herein is part of a collaborative agreement between NASA and Delft University of Technology for the advancement of composite aerospace shell structures. The work of the third and fourth authors was conducted as part of the NASA Engineering and Safety Center Shell Buckling Knockdown Factor Project, assessment number 07-010-E.

### References

- [1] Sleight, D. W., Kosareo, D. N., and Thomas, S. D., "Composite Interstage Structural Concept Down Select Process and Results," NASA NF1676L-13769, 2012, pp. 1–15.
- [2] Anon, "Buckling of Thin-Walled Circular Cylinders. NASA Space Vehicle Design Criteria," NASA SP-8007, 1965, revised 1968.
- [3] Vinson, J. R., *The Behavior of Sandwich Structures of Isotropic and Composite Materials*, Technomic, Lancaster, PA, 1999, pp. 323–330. <https://doi.org/10.1201/9780203737101>
- [4] Librescu, L., and Hause, T., "Recent Developments in the Modeling and Behavior of Advanced Sandwich Constructions: A Survey," *Composite Structures*, Vol. 48, No. 1, 2000, pp. 1–17. [https://doi.org/10.1016/S0263-8223\(99\)00068-9](https://doi.org/10.1016/S0263-8223(99)00068-9)
- [5] Hilburger, M. W., "Developing the Next Generation Shell Buckling Design Factors and Technologies," *53rd AIAA/ASME/ASCE/AHS/ASC Structures, Structural Dynamics and Materials Conference*, AIAA Paper 2012-1686, 2012. <https://doi.org/10.2514/6.2012-1686>
- [6] Schultz, M. R., Sleight, D. W., Myers, D. E., Waters, W. A., Jr., Chunchu, P. B., Lovejoy, A. E., and Hilburger, M. W., "Buckling Design and Imperfection Sensitivity of Sandwich Composite Launch-Vehicle Shell Structures," *Proceedings of American Society for Composites Technical Conference*, American Soc. for Composites, 2016, Paper 12029.
- [7] Casado, V. M., Hinsch, S., Gómez García, J., and Castro, S. G. P., "Effect of Initial Geometrical Imperfections on the Buckling Load of Cylindrical Sandwich Shells Under Axial Compression," *ESASP*, Vol. 727, 2014, p. 171.
- [8] Singer, J., Arbocz, J., and Weller, T., *Buckling Experiments: Experimental Methods in Buckling of Thin Walled Structures*, Vol. 1, Wiley, New York, 1999, pp. 217–221. <https://doi.org/10.1002/9780470172988>
- [9] Rezaeepazhand, J., Simitse, G. J., and Starnes, J. H., Jr., "Scale Models for Laminated Cylindrical Shells Subjected to Axial Compression," *Composite Structures*, Vol. 34, No. 4, 1996, pp. 371–379. [https://doi.org/10.1016/0263-8223\(95\)00154-9](https://doi.org/10.1016/0263-8223(95)00154-9)
- [10] Hilburger, M. W., Rose, C. A., and Starnes, J. H., Jr., "Nonlinear Analysis and Scaling Laws for Noncircular Composite Structures Subjected to Combined Loads," *Proceedings of the 42nd AIAA/ASME/ASCE/AHS/ASC Structures, Structural Dynamics and Materials Conference*, AIAA Paper 2001-1335, 2001. <https://doi.org/10.2514/6.2001-1335>
- [11] Marlett, K., Ng, Y., and Tomblin, J., "Hexcel 8552 IM7 Unidirectional Prepreg 190 gsm & 35% RC Qualification Material Property Data Report," National Center for Advanced Materials Performance, TR CAM-RP-2009-015, Rev. A, Wichita, KS, 2011, pp. 1–238.
- [12] Schultz, M. R., Sleight, D. L., Gardner, N. W., Rudd, M. T., Hilburger, M. W., Palm, T. E., and Oldfield, N. J., "Test and Analysis of a Buckling-Critical Large-Scale Sandwich Composite Cylinder," *Proceedings of the 58th AIAA/ASME/ASCE/AHS/ASC Structures, Structural Dynamics & Materials Conference*, AIAA Paper 2018-1693, Jan. 2018. <https://doi.org/10.2514/6.2018-1693>
- [13] Nemeth, M. P., "Nondimensional Parameters and Equations for Buckling of Symmetrically Laminated Thin Elastic Shallow Shells," NASA TM 104060, 1991.
- [14] Nemeth, M. P., "Nondimensional Parameters and Equations for Non-linear and Bifurcation Analyses of Thin Anisotropic Quasi-Shallow Shells," NASA TP-2010-216726, 2010.
- [15] Schultz, M. R., and Nemeth, M. P., "Buckling Imperfection Sensitivity of Axially Compressed Orthotropic Cylinders," *Proceedings of the 51st AIAA/ASME/ASCE/AHS/ASC Structures, Structural Dynamics and Materials Conference*, AIAA Paper 2010-2531, 2010. <https://doi.org/10.2514/6.2010-2531>
- [16] Vinson, J. R., and Sierakowski, R. L., *The Behavior of Structures Composed of Composite Materials*, Springer Science & Business Media, Dordrecht, The Netherlands, 2008, pp. 243–250. <https://doi.org/10.1115/1.3172985>
- [17] Reese, C. D., and Bert, C. W., "Buckling of Orthotropic Sandwich Cylinders Under Axial Compression and Bending," *Journal of Aircraft*, Vol. 11, No. 4, 1974, pp. 207–212. <https://doi.org/10.2514/3.59221>
- [18] Abaqus/Standard, *Software Package, Ver. 2017*, Dassault Systèmes, Waltham, MA, 2017.
- [19] Bisagni, C., "Numerical Analysis and Experimental Correlation of Composite Shell Buckling and Post-Buckling," *Composites Part B: Engineering*, Vol. 31, No. 8, 2000, pp. 655–667. [https://doi.org/10.1016/S1359-8368\(00\)00031-7](https://doi.org/10.1016/S1359-8368(00)00031-7)
- [20] Alfano, M., and Bisagni, C., "Probability-Based Methodology for Buckling Investigation of Sandwich Composite Shells with and Without Cut-Outs," *International Journal for Computational Methods in Engineering Science and Mechanics*, Vol. 18, No. 1, 2017, pp. 77–90. <https://doi.org/10.1080/15502287.2016.1276353>
- [21] Bisagni, C., "Composite Cylindrical Shells Under Static and Dynamic Axial Loading: An Experimental Campaign," *Progress in Aerospace Sciences*, Vol. 78, Oct. 2015, pp. 107–115. <https://doi.org/10.1016/j.paerosci.2015.06.004>

R. K. Kapania  
Associate Editor